

### 13. ULTRASONIC ATTENUATION MEASUREMENTS IN GABBROS FROM HOLE 735B<sup>1</sup>

David Goldberg,<sup>2</sup> Mohammed Badri,<sup>3,4</sup> and William Wepfer<sup>5</sup>

#### ABSTRACT

Compressional velocity and attenuation were measured as a function of depth in layer 3 gabbros from the recovered core at Ocean Drilling Program Site 735. High-frequency (400 kHz) acoustic transmission experiments were conducted on 117 minicore samples under room conditions of temperature and pressure on board the *JOIDES Resolution*. Although experimental errors were large in some deformed samples, the average of our measurements of  $1000/Q_p$  on these samples is  $49 \pm 32$ . Ultrasonic tests on a 1% porosity sample at elevated effective pressures from 10 up to 500 MPa showed an increase in  $V_p$  from 6.8 to 7.0 km/s and a decrease in  $1000/Q_p$  from 26 to 23. The small pressure dependence of attenuation in these low-porosity gabbros enables one to use measurements at room conditions for relative interpretation as a function of depth.

These measurements of  $1000/Q_p$  vs. depth show (1) an overall decrease in attenuation from lithologic Units II through V as a function of depth, (2) a 10-fold decrease in the average variance in the measurement in lithologic Unit II, and (3) an inverse relationship between average velocity and average attenuation. An explanation for these results is that tectonized rock fabrics have a significant effect on the measurement of attenuation and velocity. The future use of this simple shipboard operation to measure trends in attenuation as a function of depth may be effective to determine the degree of alteration and tectonism in similar, nonpressure-sensitive rocks.

#### INTRODUCTION

Laboratory elastic properties are typically measured using pulse transmission techniques at ultrasonic frequencies from 100 to 1000 kHz (Peselnick and Zietz, 1959; Hamilton, 1972; Schreiber et al., 1973; Boyce, 1974; Winkler and Plona, 1982). With these methods, group velocities are measured by pulse matching or first-break picking, and attenuation is measured from the comparison of pulses sent through a sample and through a reference. The application of the existing Hamilton-Frame ultrasonic apparatus on board the *JOIDES Resolution* can be useful to measure both elastic parameters. It is the purpose of this study to examine the elastic properties in altered and fresh gabbro samples recovered at Site 735 and to determine any systematic variations as a function of depth.

At Site 735, 500.7 m of fresh and altered gabbro was penetrated on the western flank of the Atlantis II Fracture Zone. The total core recovery in Hole 735B was 87%, with 95% recovery below 100 mbsf, which enabled sampling of the most characteristic lithologies in the hole. The gabbro section was subject to the tectonic deformations of the fracture zone, which resulted in a variety of igneous textures cut by fractures, veins, and oxide- and olivine-rich layers in the hole. The Leg 118 shipboard scientific party determined that the metamorphic and petrologic stratigraphy of the site was subdivided into six lithologic units (Robinson, Von Herzen, et al., 1989). Of particular interest was that the abundance of alteration minerals in these lithologic units (largely amphiboles) generally decreases with depth in this hole (Goldberg et al., this volume).

#### EXPERIMENTAL SETUP

The ultrasonic experiment performed on board the *JOIDES Resolution* was first used during Leg 15 of the Deep Sea Drilling Project (Fig. 1; Boyce, 1974). The general use of this Hamilton-Frame system is for measuring velocity in small core samples in the shipboard physical properties laboratory. Operating simultaneously with measurement of ultrasonic velocity, ultrasonic waveforms were recorded using an oscilloscope camera to compute the acoustic attenuation.

Piezoelectric transducers having a 400-kHz center frequency are used in the Hamilton-Frame system, one as emitter and one as receiver, on each face of the sample. The Hamilton-Frame system measures acoustic velocity through a sample placed between two rectangular (1 × 0.5 in.) barium titanate transducers in brass/epoxy cradles. A dial micrometer attached to the upper transducer is used to measure the vertical dimension of each sample. Seawater placed between the transducers and the sample ends assures a good acoustical contact. Acoustic waves 1 to 2 cm long propagate through a sample of known dimensions and at known temperature and pressure conditions. As the acoustic signal travels from the lower to the upper transducer, the compressional-wave velocity in the sample is computed from the sample height and traveltime through the sample, as recorded by a digitizing oscilloscope.

During Leg 118, the full waveform of the signal sent through the sample was simultaneously recorded using a Polaroid camera mounted over the oscilloscope screen. The time scale on the oscilloscope was fixed at 2  $\mu$ s/div or 20  $\mu$ s horizontally across the screen (approximately 5 wavelengths), and the amplitude scale and gain adjustments were fixed (usually 0.05 or 0.10 V/div) in the vertical direction. The photographed waveforms were digitized post-cruise at a sampling rate of 0.1  $\mu$ s (200 points). An example photograph and a digitized waveform of a sample from 41.3 mbsf are displayed in Figures 2A and 2B, respectively. Waveforms were recorded in a total of 117 cylindrical minicore samples, which had been kept in seawater at room temperature and pressure. On average, the samples were 20 mm long and 24.6 mm in diameter.

<sup>1</sup> Von Herzen, R. P., Robinson, P. T., et al., 1991. *Proc. ODP, Sci. Results*, 118: College Station, TX (Ocean Drilling Program).

<sup>2</sup> Borehole Research, Lamont-Doherty Geological Observatory, Palisades, NY 10964.

<sup>3</sup> King Saud University, P.O. Box 2454, Riyadh 11451, Saudi Arabia.

<sup>4</sup> Schlumberger Middle East S.A., P.O. Box 2836, Al-Khobar 31952, Saudi Arabia.

<sup>5</sup> Purdue University, West Lafayette, IN 47907.

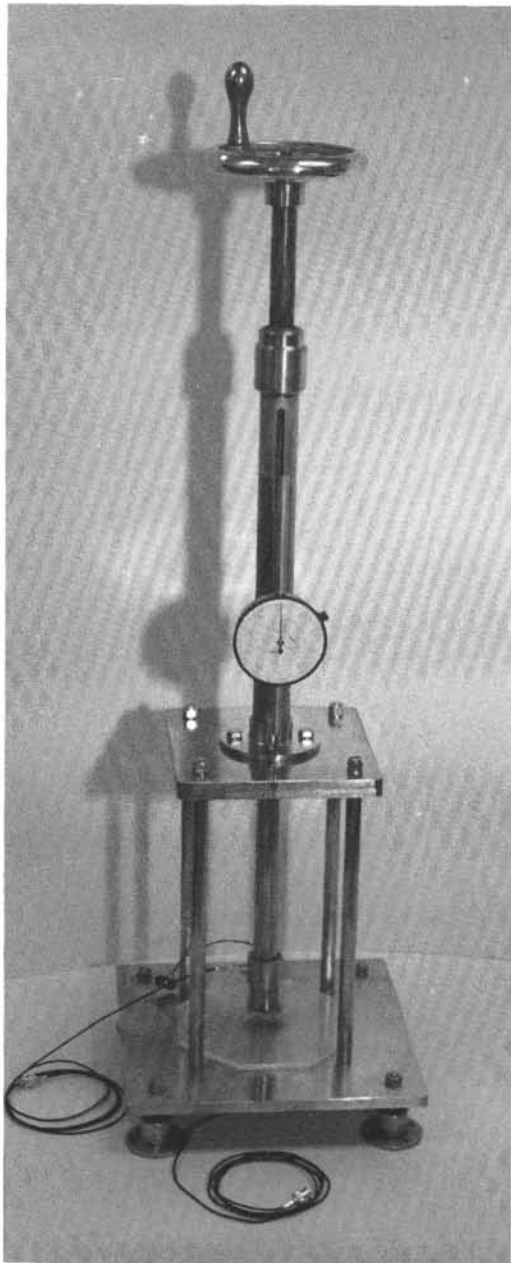


Figure 1. Photograph of the Hamilton-Frame ultrasonic apparatus on board the *JOIDES Resolution* (courtesy of D. Young, NOARL).

Attenuation was calculated by comparing the spectral decay of the received signal to a reference signal in a nonattenuating sample of the same size and shape; in this case, aluminum was used. The spectra were computed using a Fast Fourier transform (FFT) algorithm after padding the waveform with zeros to 1024 points. The corresponding Nyquist frequency and frequency interval are 5 MHz and 9.766 kHz, respectively. The frequency spectra for the sample from 41.3 mbsf is shown in Figure 3. It is clear from the figure that most of the energy has been concentrated in the frequency band between 250 and 400 kHz.

The ratio of the sample spectra divided by the reference spectra is shown in Figure 4. The attenuation coefficient  $\alpha(\omega)$  can be calculated directly from the slope of the spectral ratio by a linear regression in a frequency band from about 250 to

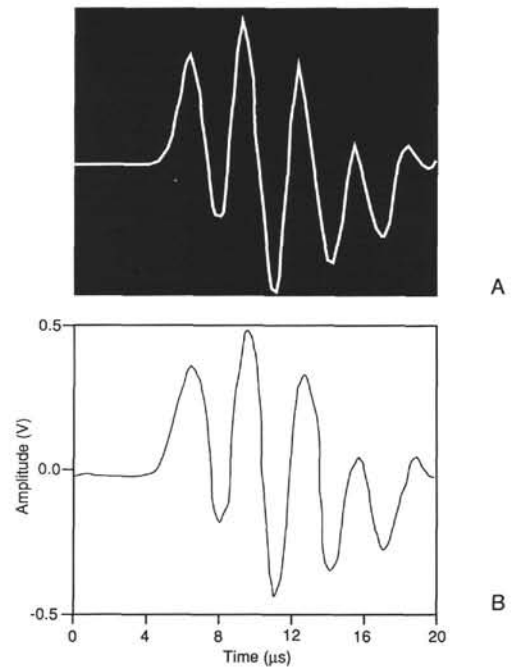


Figure 2. A. An ultrasonic waveform recorded in the laboratory on board the *JOIDES Resolution* by a Polaroid camera photograph of the oscilloscope screen. The core sample was recovered from 41.3 mbsf. B. The waveform recorded above digitized at a  $0.1\text{-}\mu\text{s}$  sampling interval.

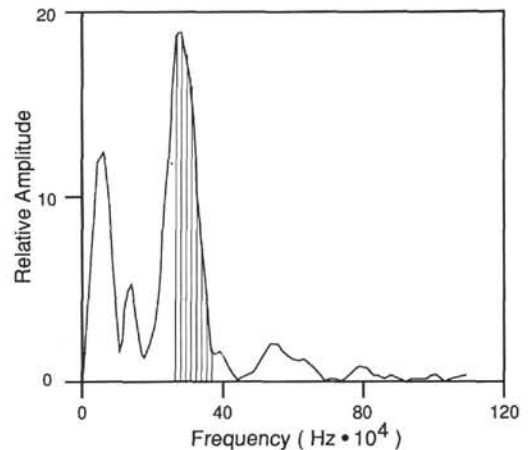


Figure 3. The Fourier transform for the waveform shown in Figure 2. The frequency interval of interest (250 to 400 kHz) has been shaded.

350 kHz.  $Q_p$  can be assumed to be independent of frequency, so that  $Q_p = \omega/2\alpha(\omega)v$  if velocity dispersion is ignored (Kolsky, 1956; Kjartansson, 1979). The linear least-squares regression enables one to estimate error in the measurement of  $Q_p$  as well. The standard deviation of the regression is used to calculate the bounds of a 95% confidence interval around the estimated slope. Thus, the variance in the measurements of  $1000/Q_p$  can be presented as an envelope around the estimated value.

### EXPERIMENTAL ERRORS

In the experimental geometry we are concerned with here, the acoustic wavelength (1.5 to 3.0 cm) is on the order

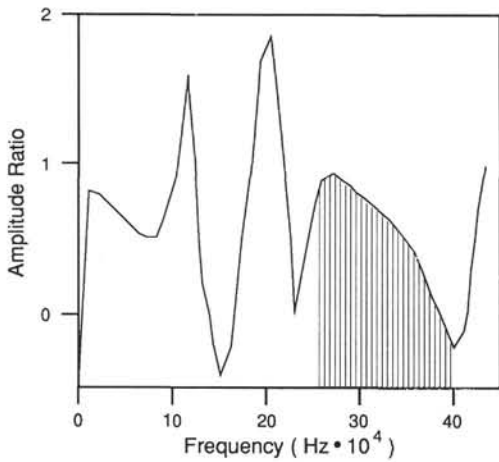


Figure 4. The ratio of spectra for the waveform in Figure 2 and a reference waveform recorded in aluminum. The frequency interval (250 to 400 kHz) used in the  $Q_p$  computation has been shaded.

of the dimensions of the transducer (0.635 cm) and sample (0.246 cm). In general, the edges of the source vibrate with slightly less amplitude than the center and create wavefronts on the transducer that are neither planar nor spherical. This phenomenon is well-known in physical acoustics as diffraction.

A number of authors have examined the problem of diffraction and calculated corrections for ultrasonic measurements of velocity and attenuation (Seki et al., 1956; Gitis and Khimunin, 1969; Papadakis and Fowler, 1971; Benson and Kiyohara, 1974; Harris, 1981). The correction is primarily a function of the Seki parameter,  $S = z\lambda/a^2$ , the distance in the  $z$ -direction between transducers normalized by the wavelength and the transducer radius. In these samples,  $V_p$  values of  $6.8 \pm 0.3$  km/s yield an average Seki parameter of 8.0 at a center frequency of 400 kHz—a regime of high  $S$ . Because the Seki parameter is large and nearly equal in the aluminum reference sample ( $S = 7.8$ ), we estimate that these corrections in this experimental configuration approximately cancel by the ratio of spectra.

Error in the measured attenuation is also induced by interfering amplitude and phase effects from reflection off the sides of the small samples. For this case, where the emitted wavelength is greater than the dimensions of the source (nonplanar wavefronts), there is likely to be energy reflected from the sides of the sample cylinder, which arrives soon after the direct compressional wave. For the idealized case of a centralized point source in a sample of radius equal to 0.635 cm and 2.0 cm long, the waveform is influenced by reflected energy between 1.5 and 2.0  $\mu$ s in the first wavelength. These residual effects on the measured attenuation are combined in an imbricated manner with intrinsic absorption and are difficult to separate. Elongating the distance of propagation (difficult in highly attenuating rocks) to reduce the diffraction effects would aggravate the problem of lateral reflections in small samples.

Although each sample was positioned similarly with respect to the transducers, diffraction and geometric effects are not exactly constant. Hence, the variations in attenuation using the ratio technique are significant, but not free of experimental error. However, the effects of source diffraction and sample geometry are less important than the intrinsic absorption of the material, and in general, attenuation measurements are reliable for lossy samples such as these. They represent the relative change in anelastic properties as a function of depth.

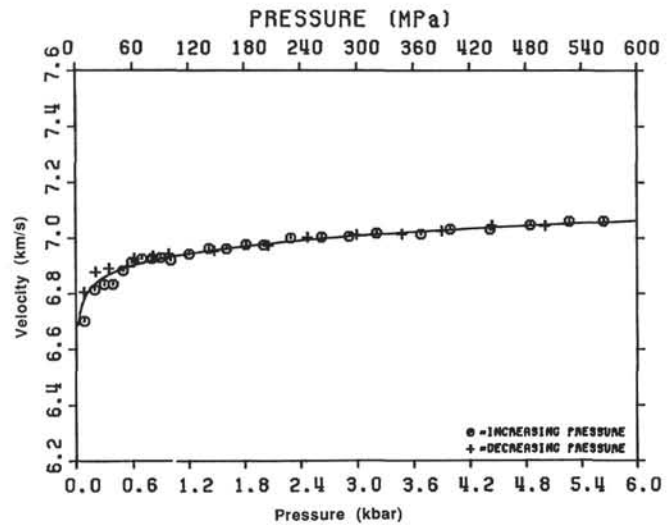


Figure 5.  $V_p$  measured in a minicube sample from 66.9 mbsf as a function of effective pressure.

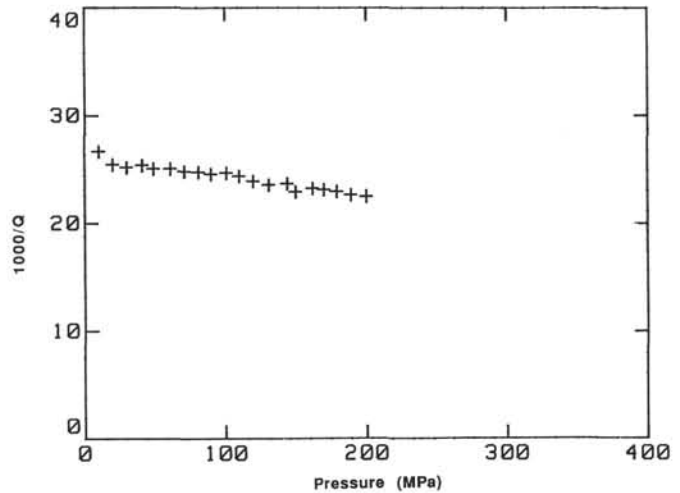


Figure 6. Measured  $1000/Q_p$  as a function of effective pressure in the same minicube sample as in Figure 5. Note that  $1000/Q_p$  has essentially negligible dependence on effective pressure in these low-porosity (0%–2%) gabbros.

### MEASUREMENTS UNDER PRESSURE

Ultrasonic tests on one sample from 66.9 mbsf were conducted at elevated effective pressures from 10 up to 500 MPa at the Purdue University Rock Physics Laboratory. The technique involves measuring a jacketed and saturated minicube sample by pulse transmission in a pressurized vessel (e.g., Winkler and Plona, 1982). The computed compressional-wave velocity ( $V_p$ ) and attenuation ( $1000/Q_p$ ) are presented in Figures 5 and 6, respectively. The data show a systematic increase in  $V_p$  from 6.8 to 7.0 km/s and a systematic decrease in  $1000/Q_p$  from 26 to 23 from 10 to 500 MPa effective pressure.

At room conditions, shipboard testing of minicore samples from 63.25 and 68.0 mbsf averaged  $6.695 \pm 0.013$  km/s and  $26.1 \pm 3.6$  for  $V_p$  and  $1000/Q_p$ , respectively. A minicore sample taken at 67.1 mbsf was unreliable owing to a confi-

dence interval more than four times in excess of the value obtained for  $1000/Q_p$  and thus was not used for comparison. For an average approximation in the interval near 67 mbsf, there is overall agreement between  $V_p$  and  $1000/Q_p$  measurements at elevated pressures and under room conditions.

Based on the test results in this moderately high (1.0%) porosity sample, the pressure dependence of attenuation appears to be negligible. This is in overall agreement with published investigations of oceanic gabbros, although other igneous rocks often do not exhibit similar behavior (e.g., Katahara et al., 1982; Wepfer and Christensen, 1989). Obviously, one cannot generalize from the results of this study to pressure-sensitive rocks, because these will not be adequately represented by properties measured at ambient conditions. Because of the low pressure sensitivity of this gabbro sample and lower-porosity gabbros throughout the hole, measurements at room conditions can be used confidently for relative interpretation between lithologic units.

**DISCUSSION OF RESULTS**

The results of the spectral ratio measurements and error estimation in Hole 735B are tabulated in the Appendix. Although experimental errors were sometimes large, the mean value of  $1000/Q_p$  ( $49 \pm 32$ ) for all 117 samples was computed. Large variances were not excluded from the data. The variation of  $1000/Q_p$  and +95% confidence interval are plotted as a function of depth in Figure 7. In Figure 8, a weak positive relationship between the confidence interval and  $1000/Q_p$  illustrates that larger variances occur for greater attenuations.

Figure 9 shows interval averages of  $V_p$ ,  $1000/Q_p$ , and 95% confidence interval (solid = 50-m intervals, short dash = 100-m intervals) and the interpreted lithology in Hole 735B. These plots show (1) an overall decrease in average attenuation from Units II

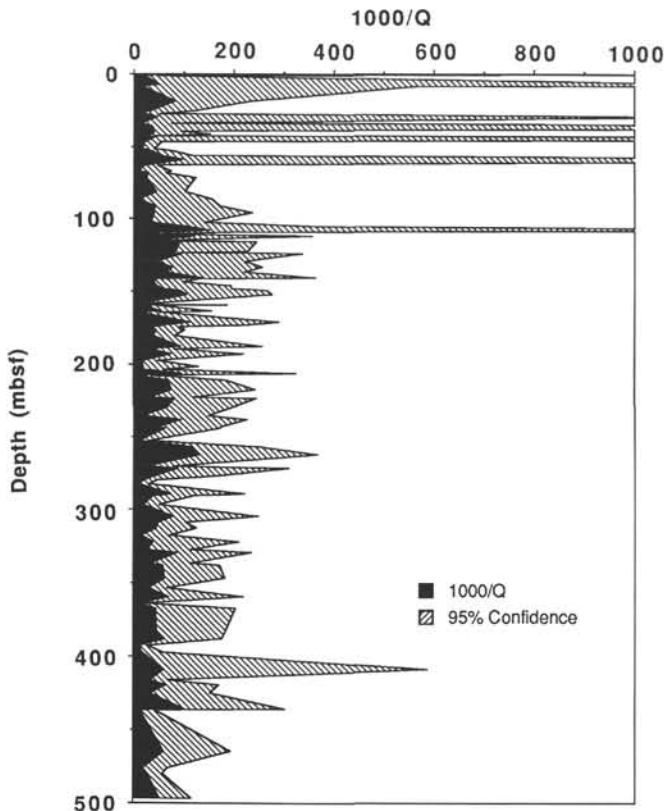


Figure 7. Variation in  $1000/Q_p$  as a function of depth at Site 735. The upper 95% confidence interval is shown by the stippled curve.

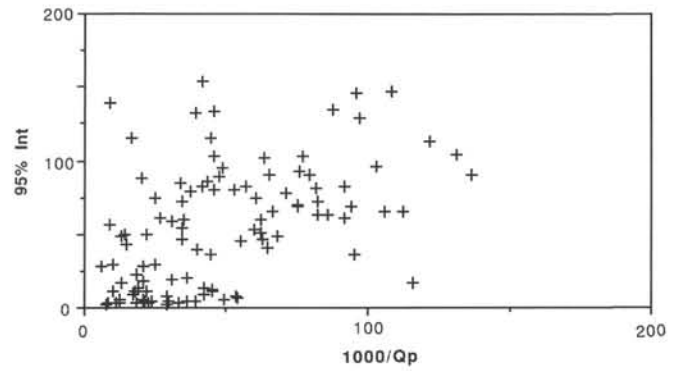


Figure 8. Crossplot of the 95% confidence interval as a function of  $1000/Q_p$ . A weak positive relationship shows that the error is greater for higher attenuations in more highly tectonized samples.

through V as a function of depth and (2) a 10-fold decrease in the average variance of the measurement (confidence interval) in Unit II at about 100 mbsf. These observations may be explained by the decreasing occurrence of altered and tectonized rock fabrics with depth, particularly in the upper 100 mbsf (Goldberg et al., this volume). The effects of severe alteration, mylonitization, and shear deformation on the measured attenuation and its variance suggest that both can be used as parameters to characterize the degree of alteration and tectonism.

An inverse relationship between  $V_p$  and  $1000/Q_p$  was also observed as a function of depth as a result of the variation in the degree of alteration and tectonism. For example, the least altered intervals in Units V and VI are the least lossy and have the highest velocities. However, point  $V_p$  estimates show no statistically important relationship with  $1000/Q_p$  (Fig. 10). Similarly, porosity measurements from core samples suggest only a weak empirical relationship with  $1000/Q_p$  (Fig. 11), supporting the generalization that the pressure dependence of attenuation is weak in these rocks (Fig. 6). Assuming that experimental errors are a small part of the variance estimates,  $1000/Q_p$  reflects the variation in alteration and tectonism in these rocks more than  $V_p$ .

**CONCLUSIONS**

Ultrasonic attenuation was measured in layer 3 gabbros from Hole 735B using the Hamilton-Frame apparatus on board the *JOIDES Resolution*. Consistent estimates of  $1000/Q_p$  were obtained and averaged  $49 \pm 32$  at ambient temperature and pressure conditions, indicating that the shipboard apparatus is a reliable tool for measuring these properties. Experimental errors in these measurements are primarily ascribed to distortion from interfering reflections from the sides of these small samples when using a 400-kHz acoustic source and can probably be significantly reduced using higher frequencies or larger samples.

Based on shore-based laboratory measurements on a 1% porosity sample, the pressure effect on attenuation appears to be negligible. Owing to the low porosity of the gabbros recovered throughout this hole,  $1000/Q_p$  is assumed to be only weakly dependent on pressure (depth), and therefore measurements at ambient conditions may be used for lithologic interpretations as a function of depth. Relative changes in  $1000/Q_p$  and independently the variance of the estimate probably represent changes in physical properties in the hole. The least altered, coarse-grained gabbros in Units V and VI are less lossy and have lower variance than highly tectonized gabbros in Unit II and above. The measurement of attenuation probably is controlled by these tectonized and metamorphic fabrics. The future use of this

shipboard technique to measure trends in attenuation as a function of depth may be effective when determining the relative degree of alteration for other Ocean Drilling Program holes drilled in nonpressure-sensitive rocks.

#### ACKNOWLEDGMENTS

Support for this project was provided by JOI/USSAC through the Ocean Drilling Program and Texas A&M University Research Foundation. Travel support for M. Badri was provided by JOI, Inc. Measurements under pressure were completed by W. Wepfer at Purdue University under contract No. N-00014-89-J-1209 to the Office of Naval Research. We greatly appreciated the efforts of R. Reynolds for presentation and A. Moser for digitization of these data.

#### REFERENCES

- Benson, G. C., and Kiyohara, O., 1974. Tabulation of some integral functions describing diffraction effects in the ultrasonic field of a circular piston source. *J. Acoust. Soc. Am.*, 55:184-185.
- Boyce, R. E., 1974. Physical properties. In Edgar, N. T., Saunders, J. B., et al., *Init. Repts. DSDP*, 15: Washington (U.S. Govt. Printing Office), 1119-1129.
- Gitis, M. B., and Khimunin, A. S., 1969. Diffraction effects in ultrasonic measurements (review). *Sov. Phys.-Acoust.*, 14:413-431.
- Hamilton, E. L., 1972. Compressional wave attenuation in marine sediments. *Geophysics*, 37:620-646.
- Harris, G. R., 1981. Review of transient field theory for baffled planar piston. *J. Acoust. Soc. Am.*, 70:10-20.
- Katahara, K. W., Manghnani, M. H., Devnani, N., and Tittmann, B. R., 1982. Pressure dependence of  $Q$  in selected rocks. *Adv. Earth Planet. Sci.*, 12:147-158.
- Kjartansson, E., 1979. Constant  $Q$ -wave propagation and attenuation. *J. Geophys. Res.*, 84:4737-4748.
- Kolsky, H., 1956. The propagation of stress pulses in viscoelastic solids. *Philosoph. Mag.*, 1:693-710.
- Papadakis, E. P., and Fowler, K. A., 1971. Broad-band transducers: radiation field and selected applications. *J. Acoust. Soc. Am.*, 50:729-745.
- Peselnick, L., and Zietz, I., 1959. Internal friction of fine-grained limestones at ultrasonic frequencies. *Geophysics*, 24:285-296.
- Robinson, P. T., Von Herzen, R., 1989. *Proc. ODP, Init. Repts.*, 118: College Station, TX (Ocean Drilling Program).
- Schreiber, E., Anderson, O. L., and Soga, N., 1973. *Elastic Constants and Their Measurements*: New York (McGraw-Hill).
- Seki, H., Granato, A., and Truell, R., 1959. Diffraction effects in the ultrasonic field of a piston source and their importance in the accurate measurement of attenuation. *J. Acoust. Soc. Am.*, 28:230-238.
- Wepfer, W. W., and Christensen, N. I., 1989.  $Q$  anisotropy in metamorphic rocks. *EOS, Trans. Am. Geophys Union*, 70:458.
- Winkler, K., and Plona, T. J., 1982. Techniques for measuring ultrasonic velocity and attenuation spectra in rocks under pressure. *J. Geophys. Res.*, 87:10776-10780.

Date of initial receipt: 11 July 1989

Date of acceptance: 31 January 1990

Ms 118B-143

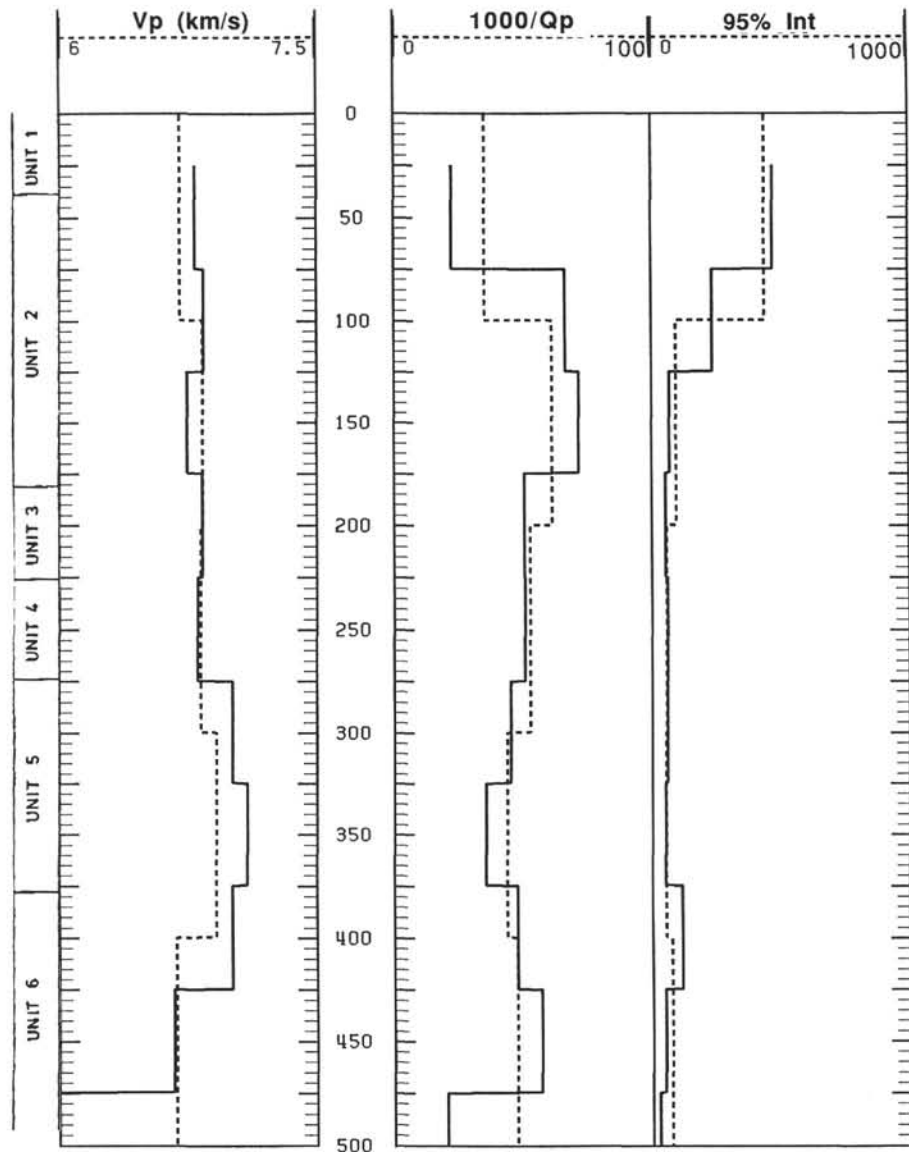


Figure 9. Averages of  $1000/Q_p$ ,  $V_p$ , and 95% (confidence) interval over 50-m intervals at Site 735. Below 100 mbsf, error values decrease by a factor of 10, and  $V_p$  is inversely correlated to  $1000/Q_p$ . The highest velocity and lowest attenuation occur in Unit V near 350 mbsf.

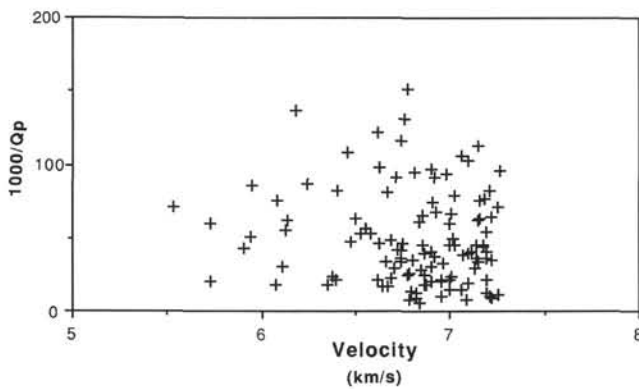


Figure 10. Crossplot of  $1000/Q_p$  as a function of  $V_p$  for all minicore samples.

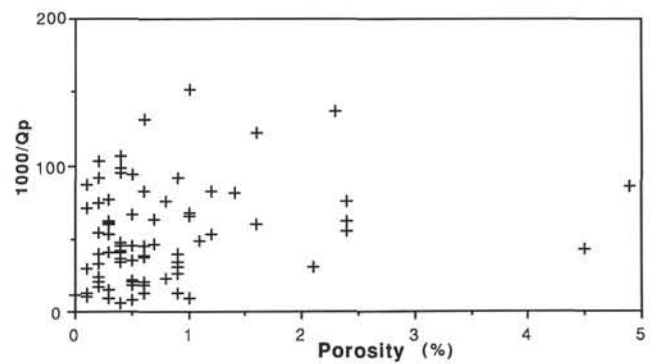


Figure 11. Crossplot of  $1000/Q_p$  as a function of core porosity for all minicore samples. A weak positive relationship is suggested from these data.

APPENDIX

Table of velocity ( $V_p$ ), attenuation ( $1000/Q_p$ ), 95% confidence interval ( $1000/Q_p$ ), and the Seki parameter ( $S$ ) for 117 samples measured under shipboard (room) conditions from Hole 735B. Mean values for these gabbros are  $V_p = 6.8$  km/s and  $1000/Q_p = 49$ .

Depth	Velocity	1000/Q	95% Int	S
0.15	5.533	70.67	1290.43	5.20
1.37	6.397	21.59	3.75	7.08
7.62	5.938	50.77	1186.77	7.04
7.92	6.376	23.31	1221.39	8.63
8.99	6.078	17.91	529.52	7.45
19.05	6.400	82.16	72.63	7.07
25.15	6.657	34.18	54.74	7.75
26.67	6.998	14.22	50.27	8.94
27.58	7.005	23.89	4.53	8.85
29.72	6.752	46.49	1044.08	8.58
34.44	6.823	12.90	48.08	8.77
36.42	6.744	36.53	2212.20	8.04
39.78	6.743	41.98	9.30	9.67
41.30	6.913	37.02	78.65	8.64
42.52	6.900	20.88	3.03	8.70
43.28	7.193	40.86	2652.20	8.29
47.09	7.191	21.99	11.37	8.52
51.51	6.345	18.48	3.28	6.34
52.88	7.188	35.87	4.87	8.17
55.93	7.195	54.02	6.69	7.90
58.98	6.621	98.16	1815.31	7.30
63.25	6.686	22.43	3.00	7.82
67.06	6.821	8.96	56.80	7.15
67.97	6.704	29.79	4.20	7.96
71.32	6.867	24.56	74.16	8.13
80.92	7.142	44.87	11.91	7.37
86.26	7.220	8.96	138.71	9.62
91.14	5.901	43.14	85.94	6.59
95.86	7.114	41.22	154.02	8.85
102.26	7.218	34.60	72.18	8.58
105.16	6.453	108.49	146.52	7.60
107.90	6.778	151.87	1268.52	7.25
108.97	6.690	48.71	95.12	7.26
110.19	6.952	20.87	5.13	8.36
112.01	6.613	121.64	113.25	7.68
114.91	7.255	11.46	3.82	8.87
116.13	6.921	91.97	60.48	7.74
122.38	7.213	82.37	62.90	8.16
123.14	6.955	21.73	49.68	8.35
123.75	7.259	95.73	146.32	7.35
129.08	7.173	45.48	132.86	8.85
133.50	7.183	76.90	102.92	8.27
136.25	6.852	64.99	90.70	8.71
140.82	6.178	136.89	89.90	7.68
141.12	6.799	34.73	60.22	8.42
143.41	6.724	41.92	13.56	8.02
146.15	7.026	45.39	103.11	8.13
148.13	6.556	56.87	82.07	8.20
149.20	6.712	91.92	82.70	8.20
151.64	7.056	105.77	65.34	8.59
158.34	6.786	7.69	2.45	7.83
159.26	6.577	52.73	79.93	8.26
159.56	6.671	17.14	9.47	8.18
163.37	6.125	54.87	45.75	7.21
163.83	7.214	10.19	29.86	8.39
170.38	7.148	112.57	65.56	8.70
172.67	7.159	63.04	101.15	7.68
174.35	7.138	35.94	20.46	9.04
176.17	6.855	45.02	11.40	8.09
179.83	6.864	39.01	4.71	8.18
187.45	6.983	94.16	69.40	7.30
189.28	6.109	30.60	19.08	6.99
193.09	6.079	75.38	69.18	7.52
197.21	6.863	17.52	11.46	8.71
201.17	6.899	20.27	88.66	8.04

Depth	Velocity	1000/Q	95% int	S
203.76	6.999	20.96	17.69	8.33
206.04	6.897	96.89	128.93	8.64
207.26	6.837	5.91	28.05	7.71
211.07	6.924	67.88	48.56	9.20
217.63	7.156	75.66	92.14	8.42
222.66	6.901	30.79	58.45	7.40
223.72	6.671	81.82	81.63	8.14
229.51	7.010	66.46	65.35	8.40
235.31	6.640	16.79	115.31	8.13
238.35	6.809	95.08	35.68	9.52
243.38	6.624	45.81	80.28	8.10
243.99	6.498	62.92	46.04	7.31
253.14	6.822	12.56	5.33	8.21
257.10	6.742	115.89	16.41	8.56
262.28	6.754	131.18	103.62	6.78
270.36	6.773	24.70	29.27	9.18
271.58	6.240	87.56	134.86	7.91
277.06	6.896	41.23	82.99	7.67
279.96	6.617	21.15	5.08	7.61
282.40	6.951	10.25	11.06	8.44
289.26	6.907	75.04	70.52	8.38
290.63	7.099	39.46	39.95	8.74
296.27	7.099	18.82	14.05	8.05
304.50	7.025	79.06	90.40	8.67
308.76	7.016	49.40	5.52	8.25
312.72	6.994	44.64	36.23	8.28
316.99	7.061	14.80	42.70	8.02
322.17	7.071	38.92	131.75	8.02
327.36	6.785	26.49	61.06	7.79
329.34	5.948	85.57	63.54	5.99
336.80	7.145	34.09	46.18	9.97
338.18	6.993	59.62	52.83	8.48
347.01	6.133	61.90	59.39	7.32
353.26	7.128	29.01	8.04	8.39
359.36	7.251	70.81	78.19	8.33
364.24	7.089	8.05	3.44	9.56
367.28	7.173	44.59	115.30	7.64
382.98	6.469	47.30	89.49	7.55
388.01	7.148	62.09	51.33	7.92
392.73	7.195	12.65	3.65	8.15
397.46	6.872	18.62	22.51	8.78
408.74	6.837	60.56	465.49	8.64
416.66	6.957	33.12	3.03	8.42
419.71	7.220	64.74	41.21	8.93
425.35	6.741	33.92	84.53	7.46
435.56	7.094	102.82	95.87	8.73
436.17	6.790	13.09	16.91	7.79
464.21	7.062	52.08	11.87	8.29
464.21	5.731	60.15	74.23	6.28
476.10	5.731	20.56	27.78	6.28
479.60	6.850	28.73	1.79	8.08
496.67	6.526	53.48	8.22	8.53
MEANS	6.798	49.14	165.91	8.07
STDEV	0.369	32.03	417.85	0.77